Performance of reinforced concrete flat slabs having GFRP gratings

Haitham M.F. Mostafa, Ahmed A. Mahmoud*, Tarek S. Mostafa, Ahmed N. M. Khater
Benha University, Faculty of Engineering at Shoubra, Cairo, Egypt
haiythaam@yahoo.com, https://orcid.org/0009-0004-2287-7564
ahmed.ahmed@feng.bu.edu.eg, http://orcid.org/0000-0003-2306-5950
tarek.mohamed@feng.bu.edu.eg, http://orcid.org/0000-0002-0015-9113
ahmed.khater@feng.bu.edu.eg, http://orcid.org/ 0000-0003-4528-8979

Citation: Mostafa, H. M. F., Mahmoud, A.A., Mostafa, T. S., Khater, A. N. M., Performance of reinforced concrete flat slabs having GFRP gratings, Frattura ed Integrità Strutturale, 67 (2024) 240-258.

Received: 10.09.2023
Accepted: 04.12.2023
Online first: 08.12.2023
Published: 01.01.2024

KEYWORDS. Punching shear, GFRP gratings, Flat slab, Numerical analysis, Experimental investigation, Reinforced concrete.

INTRODUCTION

The approach of utilizing a fiber-reinforced polymer (FRP) has gained the most attention as one of the most efficient shear reinforcements due to the characteristics of FRP, such as its lightweight, high tensile strength, and ability to be created in different forms. The use of FRP sheets, laminates, strips, and rods for strengthening and reinforcing concrete structures is widespread. Limited research investigated GFRP with gratings shape performance characteristics and considered the effect of GFRP gratings as punching shear resistance. Bank et al. [1] produced full-size tests on concrete slab bridge decks reinforced by pultruded glass fiber gratings. The investigation has demonstrated that FRP gratings may be viable reinforcements for bridge deck slabs. Bank et al. [3] conducted an experimental and analytical investigation to study the effect of pultruded FRP grating cages on reinforced concrete members, and according to the findings of the pilot study, further improvement of FRP grating cages for reinforced concrete appears to be justified. Biddah [2] tested the application of replacing the steel reinforcement of concrete slabs with pultruded GFRP grating sections as a structural reinforcement for the bridge decks and studied experimentally the mechanical and chemical properties of GFRP gratings. The test results revealed that pultruded fiberglass grating may significantly enhance the capacity of concrete slabs. Gattescoa et al. [4] discussed experimentally and analytically the results on molded GFRP gratings at full scale with different boundary

conditions to study the gratings bending performance and produced a valuable model for future research on more complicated combinations.

On the other hand, numerous previous kinds of research have been devoted to studying the enhancement of using FRP material in various shapes. Swamy and Ali [5] investigated the influence of fiber reinforcement on the deflection and punching shear strength characteristics. The fibers have been utilized across the slab or in the punching shear zone over the column head, and comparison tests were conducted on connections with bent steel bars. The results demonstrated that fibers decrease deformations throughout all phases of loading, enhance ultimate punching shear stresses, and result in ductile shear failures. Ospina et al. [6] conducted four tests to compare the behavior of steel and FRP-reinforced slab column connections. The primary variables included slab reinforcement material (steel or GFRP), reinforcing mat type (individual bars or two-dimensional grid), and slab reinforcement ratio. The experimental evidence revealed that the behavior of an FRP-reinforced slab-column connection is influenced by the elasticity of the reinforcing mat and the quality of its bond with the concrete. Mu and Meyer [7] conducted an experimental investigation on fiber-reinforced glass aggregate concrete slabs subjected to a central patch load. The effects of fiber type, shape, and volume ratio on the two-way bending behavior and punching shear capacity of glass concrete slabs were studied. The results demonstrated that fiber mesh is significantly more effective in bending than randomly distributed fibers; however, randomly distributed fibers are marginally more effective in punching shear. Zhang et al. [8] compared three specimens of one-way concrete slabs with CFRP grid reinforcement to a specimen reinforced with steel bars.

Dimitrios et al. [9] evaluated the punching shear capacity of internally FRP-reinforced slab column connections without shear reinforcement based on a simple analytical model and presented a proposed equation, which provided a practical and accurate methodology for the punching capacity analysis of slabs enhanced with FRP bars or grids. Esfahani et al. [10] studied the punching shear strengthening of flat slabs using Carbon Fiber Reinforced Polymer (CFRP) sheets. The test results revealed that using CFRP sheets as flexural reinforcement in addition to steel reinforcing bars improved slab punching shear strength. This increase has the potential to be considerable for slabs composed of high-strength concrete with a low steel reinforcing ratio. Said et al. [11] executed an experimental and numerical study on thirteen lightweight concrete flat slab specimens to increase punching shear resistance utilizing various reinforcing approaches. Hemzah et al. [12] studied the punching shear behavior of ten slab specimens reinforced by double or single layers of CFRP or steel bars with varied parameters. Analytical modeling for the tested specimens was carried out using the finite element program ABAQUS. A punching shear formula was presented to estimate the ultimate punching shear for concrete slabs, which gave close results compared to the experimental, numerical, and previous studies. Kim and Lee [13] examined nine specimens strengthened with a GFRP vertical grid. Mohmmad et al. [14] studied the punching shear behavior of geopolymer concrete two-way slabs reinforced by FRP bars under monotonic and cyclic loadings. The results revealed that increasing both the concrete strength and reinforcing ratio provided a larger punching shear capacity and reduced deflections under cyclic and monotonic loading. Furthermore, the punching shear performance of geopolymer concrete slabs was discovered to be superior to that of regular concrete. Mahmoud et al.[15- 16] studied experimentally and numerically the behavior of reinforced concrete slabs under punching loads. Minh and Rovňák [17] studied experimentally six slab column connections at large scale reinforced by GFRP and steel bars with different tensile steel ratios. A new empirical equation for calculating the punching shear resistance of internal GFRP-reinforced slab-column connections was proposed. The results showed that increasing the GFRP reinforcement ratio in the investigated slabs improves punching shear resistances by up to 36% and decreases deflections by up to 35%. Compared to previous formulations, the suggested empirical method gives more accurate predictions of the punched shear resistance of internal FRP-reinforced slab column connections throughout the whole range of examined parameters. Elmoien et al. [18] studied experimentally and analytically the punching behavior of internally strengthened R.C. circular flat slabs using different techniques.

The present study aims to evaluate experimentally and numerically the use of molded Glass Fiber Reinforced Polymer (GFRP) gratings to increase the punching shear resistance of concrete flat slab column connections. The suggested GFRP grating can be implemented in practical applications such as in RC flat slabs, in foundations in the zone of the column, and in RC plie capes, and can be used as shear web reinforcement for beams.

EXPERIMENTAL PROGRAM

Description of tested specimens

The experimental program consists of seven square slab column connection specimens, measuring 1100×1100 mm with a thickness of 150 mm, constructed and tested in the concrete laboratory at the Faculty of Engineering Cairo University, and the specimens were designed to fail in punching. All columns were cast monolithically at the center

of the slab with a 300-mm square section and extended above the slab by 300-mm. The main flexural reinforcement of the slab was uniformly spaced using 5 Φ 16 bars in both directions as a bottom reinforcement mesh (on the tension side) and 5 Φ 12 bars in both directions as a top reinforcement mesh (on the compression side). The column is reinforced with 8 Φ 12 with three stirrups of 8 mm diameter. Figs. 1, 2, and 3 illustrate the typical concrete dimensions, photographs, and steel reinforcement for the tested specimens.

The tested specimens were divided into five groups to investigate the studied parameters, as shown in Tab. 1. The first group consists of two specimens, SP01 without gratings and SP02 with GFRP gratings at the mid-slab thickness, with dimensions of 700×700×15 mm, to investigate the effect of the proposed GFRP gratings on punching shear behavior. The second group consists of three specimens, SP02, SP03, and SP04, each with GFRP gratings with dimensions 700×700×15 mm at the mid, top, and bottom of the slab thickness, to investigate the effect of gratings location throughout the slab thickness. In the third group, two specimens are utilized to examine the effect of grating numbers. Specimen SP02 has a single 700×700×15 mm GFRP grating installed at the middle of the slab thickness, whereas SP05 has two GFRP gratings of the same dimensions attached to the top and bottom of the steel reinforcements of the slab. Specimens SP02 and SP06 in the fourth group have the same GFRP grating dimension of 700×700 mm but with a varied thickness in the mid-slab thickness (15 mm for specimen SP02 and 38 mm for specimen SP06) to study the effect of grating thickness. The fifth group consists of two specimens, SP02 and SP07, with different dimensions of GFRP grating, with dimensions of 700×700×15 mm for specimen SP02 and 800×800×15 mm for specimen SP07, to examine the effect of grating dimensions.

Mixture composition

The materials used in the experimental program include dolomite (coarse aggregate), sand (fine aggregate), cement, reinforcement steel, and GFRP gratings. Tests were carried out to determine the mechanical and chemical properties of the used materials according to ACI 318-2019 [19], ASTM C469/C469 M-14 [21], ASTM C496-96 [22], and ASTM C39/C39 M-14 [23].

Concrete components

The cement used in this study was ordinary Portland cement (OPC), which is manufactured locally and complies with ACI 318-2019 [19]. Crushed brown dolomite (coarse aggregate) and sand (fine aggregate) from local sources were used. The ratio between the sand and the coarse aggregate was taken as 1:1.65 (by weight) in all mixes of all tested slabs. Clean, potable water free from impurities was used for mixing the concrete and curing it after casting. The water-cement ratio was designed to be 0.54 (by weight). The concrete mix was designed to reach a compressive strength of 25 MPa after 28 days.

Reinforcing steel

High-tensile steel bars are used with a yield strength of 486 MPa and an ultimate strength of 579 MPa for a 12 mm diameter and a yield strength of 444 MPa and an ultimate strength of 553 MPa for a 16 mm diameter. Fig. 4 illustrates the stress-strain relationship for reinforcement steel bars.

GFRP gratings

Seven molded GFRP gratings from the Egypt FRP composite factory according to ECP-208 [17] with different dimensions and thicknesses were used in this research to cover all the experimental parameters. The gratings were manufactured by interweaving continuous, thoroughly wetted fiberglass strands with thermosetting Calcium Carbonate, and Hardener Peroxide. The standard resin system is GP polyester resin with moderate corrosion resistance. Standard spacing dimensions and web-size for GFRP gratings with a thickness of 38 mm and 15 mm are illustrated in Fig. 5.

Load bearing test under central line load according to ASTM [21] was performed for two gratings specimens with dimensions of 200×1000×15 mm and 500×500×38 mm to determine the central deflection and strain in each grating and evaluate the elastic modulus corresponding to deflections measured in the mechanical experiment. Linear Variable Differential Transducer (LVDT) and electric strain gauges were used to measure the central deflection and strains of gratings. From the results, the elastic modulus for gratings with 38 mm and 15 mm thickness is approximately equal to 12 GPa and 6 GPa, respectively. The experimental setup and stress-strain curves for both gratings specimens are presented in Figs. 6 and 7.

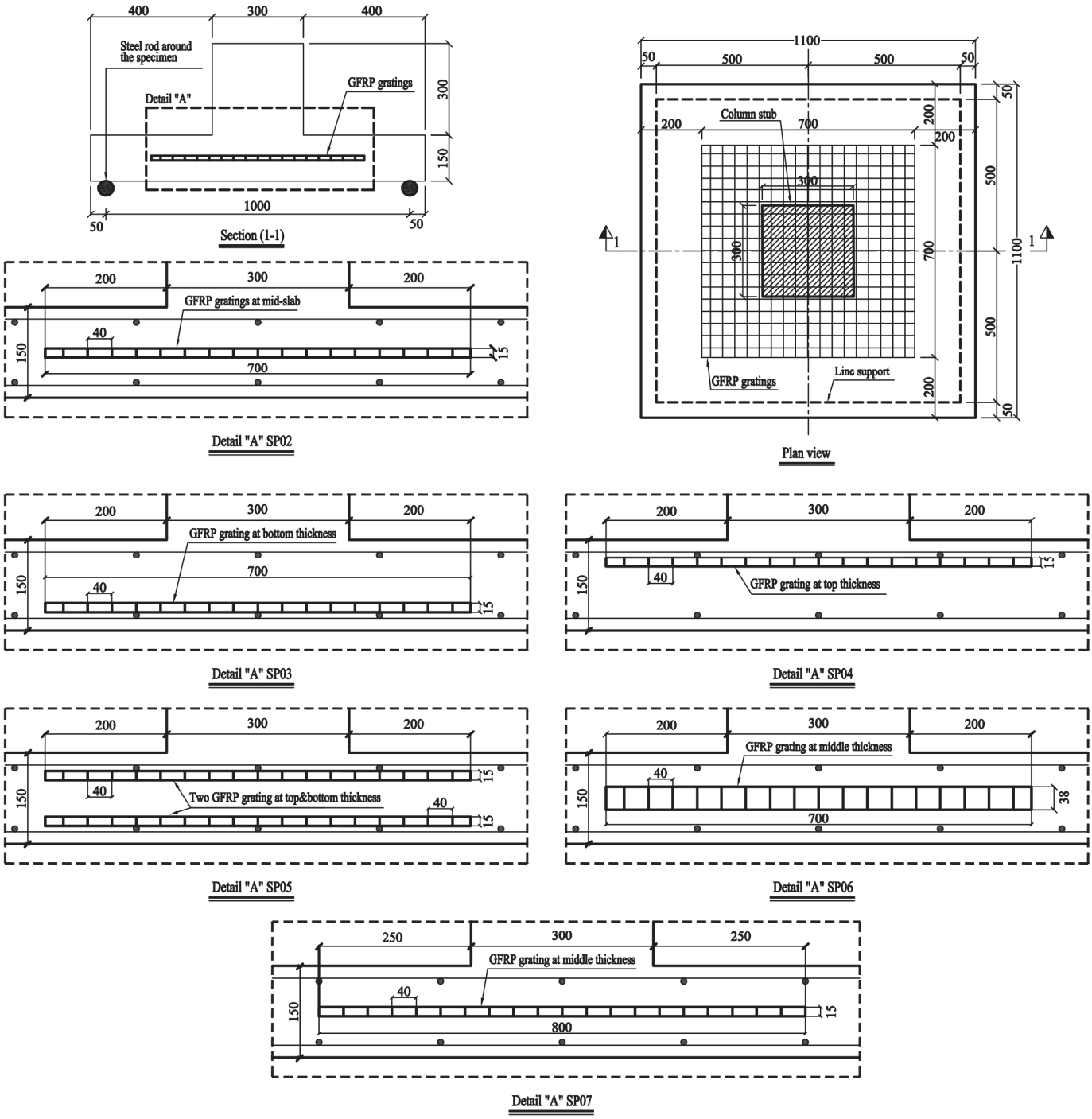

Figure 1: Typical concrete dimensions for the tested specimens (all dimensions are in mm).

Figure 2: Tested specimen's preparation, reinforcement, and cast

Specimen model	Group No.	GFRP grating dimensions (mm)	Grating position through the slab thickness	Number of gratings	Grating thickness (mm)	Notes
SP01	Control specimen	Without gratings	Without gratings	-	Without gratings	Control specimen
SP01	1	Without gratings	Without gratings	-	Without gratings	Effects of using the gratings
SP02		700x700	Middle	1	15	
SP02		700x700	Middle	1	15	Effects of grating position on the slab thickness
SP03	2	700x700	Bottom	1	15	
SP04		700x700	Top	1	15	
SP02	3	700x700	Middle	1	15	Effect of the number of gratings
SP05		700x700	Top and bottom	2	15	
SP02	4	700x700	Middle	1	15	Effect of grating thickness
SP06		700x700	Middle	1	38	
SP02	5	700x700	Middle	1	15	Effect of grating dimensions
SP07		800x800	Middle	1	15	

Table 1: Studied parameters.

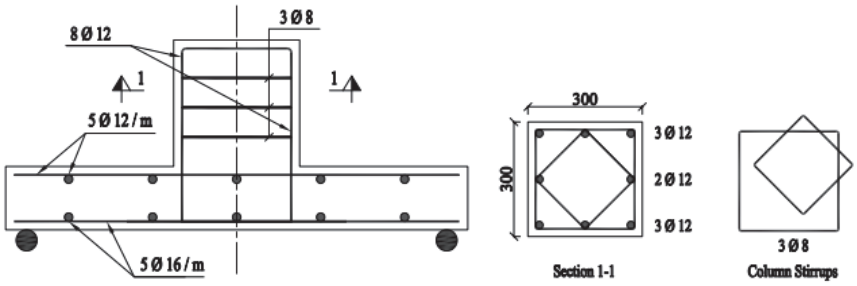

Figure 3: Typical reinforcement details for the tested specimens (all dimensions are in mm).

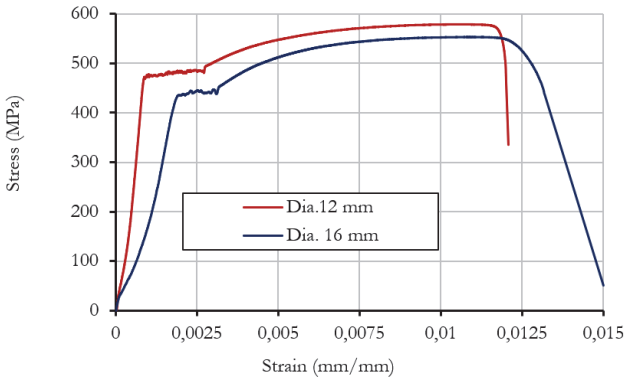

Figure 4: Stress-strain relationship for reinforcing steel bars.

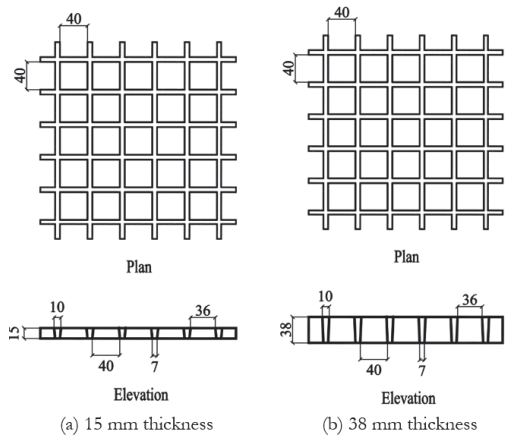

Figure 5: Dimensions of grating with thicknesses 15 and 38 mm.

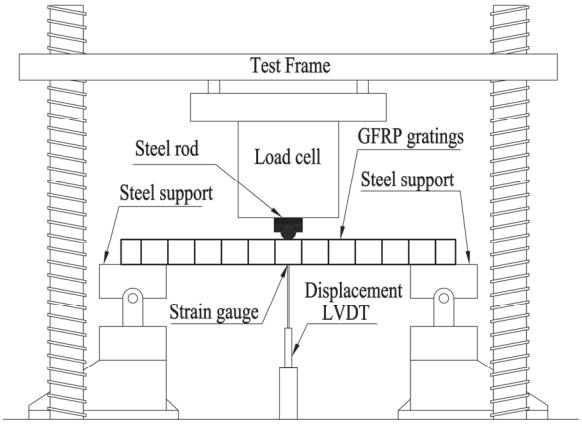

Figure 6: Load bearing test set up for GFRP gratings specimens

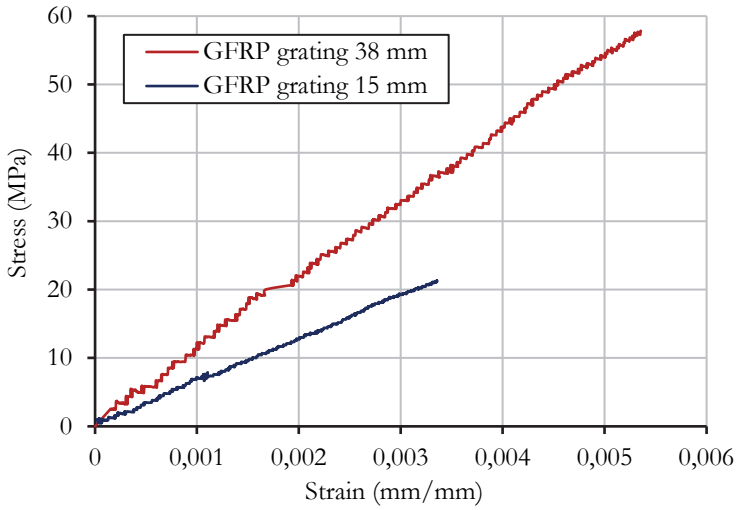

Figure 7: Experimental stress-strain curves for GFRP gratings specimens

Test setup

Fig. 8 shows the typical test setup for the specimens. The load was controlled by a load cell with a capacity of 1000 kN. The load cell was attached to the testing frame by plates and high-strength steel bolts. The specimens were supported all around on steel rods of 25 mm diameter welded to a steel rigid-rig frame. The statical load was applied monotonically as a displacement control with a rate of 1.0 mm/min. At each load increment, the cracks were marked, and measurements of

electrical strain gauges with a 10 mm length and 120 Ω resistance were recorded to determine the strains in the concrete top surface (compression side), the flexural reinforcement, and the GFRP gratings. Fig. 9 showed the arrangement of strain gauges for all specimens.

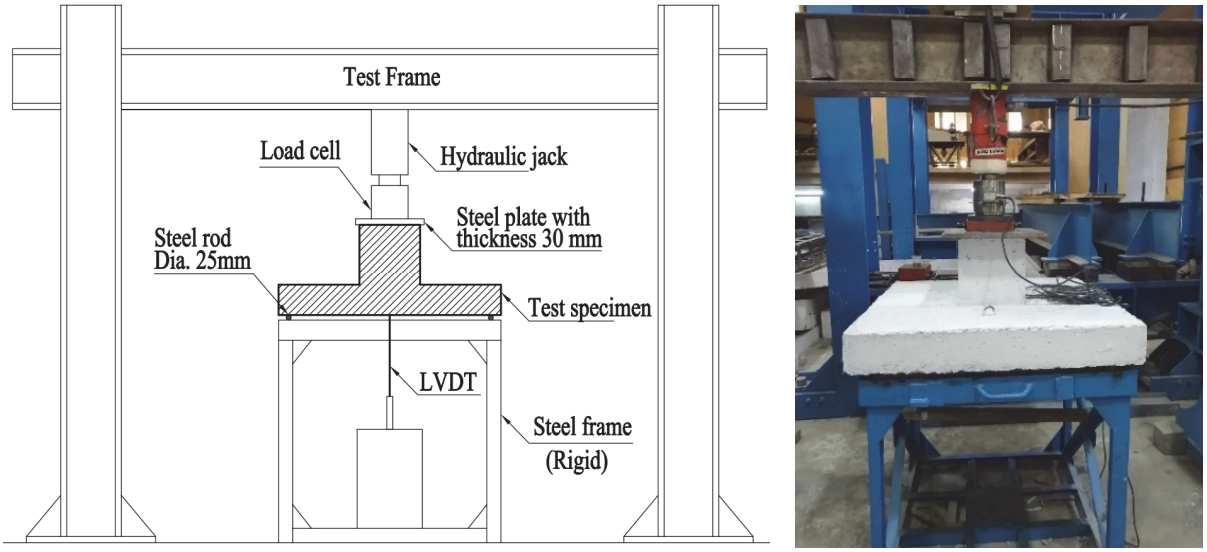

Figure 8: Test setup.

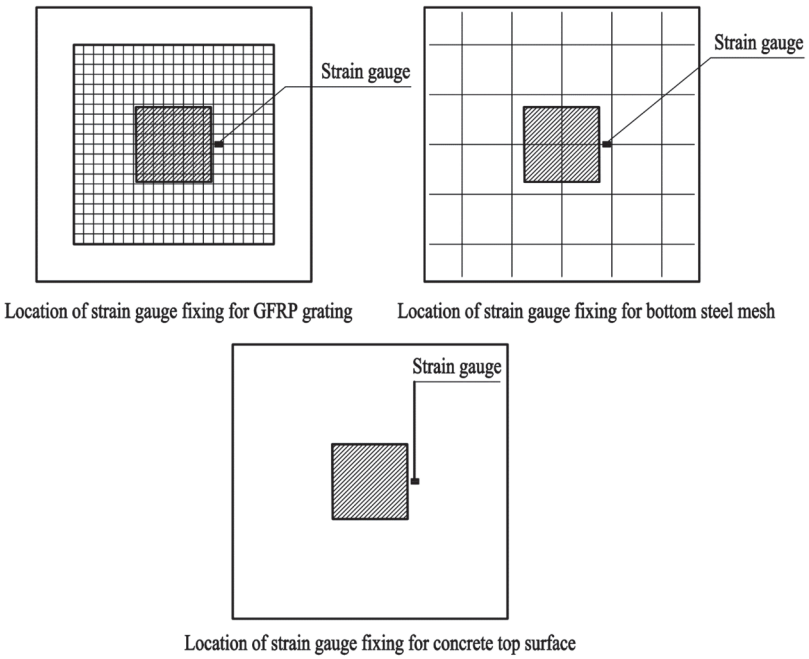

Figure 9: Arrangement of strain gauges for all specimens

Analysis of the experimental results

The first crack load and crack patterns

Fig. 10 shows the typical crack patterns for the tested slabs. In general, the crack patterns of all specimens subjected to concentric loading were symmetric about both specimen axes. For specimen SP01 without GFRP gratings, perpendicular cracks started to appear at the column face at a load level of 100.0 kN. Small radial and tangential cracks appeared towards the column corners at a load level of 120.0 kN. A few radial cracks appeared as the load increased,

while the primary cracks widened. The radial cracks extended significantly at a load level of 150.0 kN. At a load level of 175.0 kN, some tangential cracks started to appear around the column face. Then, at a load level of 274.25 kN, a sudden brittle failure occurred (take a short time), forming a truncated cone in the slab. During the failure stage, some of the concrete cover on the bottom surface split off the slab. Fig. 10(a) depicts the crack pattern of specimen SP01.

For the specimens with integrated GFRP gratings, perpendicular cracks started at the bottom surface (on the tension side) around the column at a load level of 30% of the failure load. Small radial and tangential cracks were observed around the column corners. As the load progressed, more radial cracks appeared, whereas the widths of the tangential cracks increased. At a load level of 40% of the failure load, the radial cracks expanded significantly. When approaching 60% of the failure load, many tangential cracks appeared around the GFRP gratings, and major tangential cracks developed. At the failure load, the slab experienced sudden brittle failure (taking a short time after reaching the failure load) and the formation of a truncated cone close to the line support. At the level of the flexural reinforcement, the punching shear cracks converted into a horizontal separation that followed the reinforcement to the slab's edges. Fig. 10(b) depicts a typical crack pattern of specimens with integrated GFRP gratings.

Tab. 2 presents the test results as (1) first crack loads (P_{cr}); (2) failure loads (P_f); (3) deflection at failure load (ε_f); (4) concrete strain at failure (ε_{cf}); (5) steel strain at failure (ε_{sf}); (6) GFRP gratings strain at failure (ε_{gf}); and (7) toughness (T) for all tested specimens. Tab. 3 presents the test results compared to the control specimen, SP01.

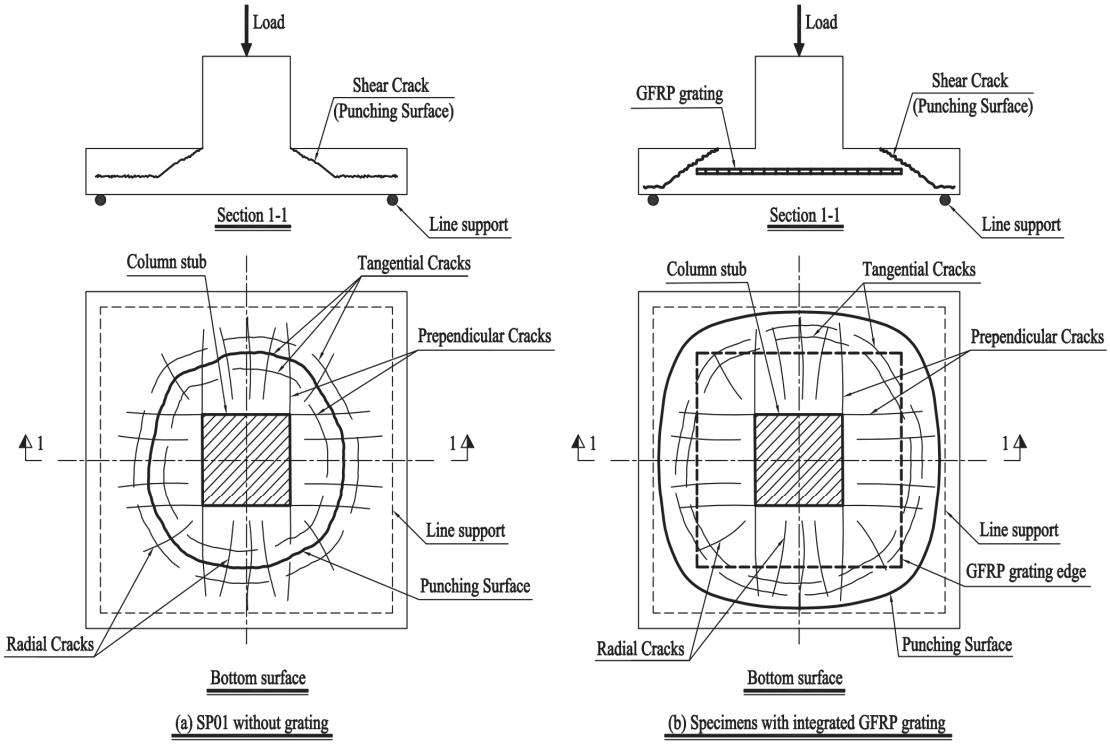

Figure 10: Typical cracking pattern for the tested slabs.

Specimen Number	P_{cr} (kN)	P_f (kN)	Δ_f (mm)	ε_{cf} (10^{-3})	ε_{sf} (10^{-3})	ε_{gf} (10^{-3})			T kN/mm
						Top	Middle	Bottom	
SP01	100.47	275.62	12.39	2.28	2.20	N.A.	N.A.	N.A.	1962.76
SP02	110.27	300.52	13.98	2.04	2.32	N.A.	2.78	N.A.	2212.60
SP03	110.14	327.81	13.48	2.49	2.08	N.A.	N.A.	1.88	2251.67
SP04	110.38	331.90	13.27	2.25	1.93	2.34	N.A.	N.A.	2318.58
SP05	110.08	324.74	13.32	2.32	2.23	2.00	N.A.	1.63	2157.82
SP06	111.54	351.87	13.18	2.42	2.29	N.A.	1.96	N.A.	2377.21
SP07	110.76	332.58	14.52	2.29	2.42	N.A.	2.95	N.A.	2697.67

Table 2: The experimental results of the tested slabs

Specimen Number	$P_{cr}/P_{cr\,SP01}$ (%)	$P_f/P_{f\,SP01}$ (%)	$\Delta_f/\Delta_{f\,SP01}$ (%)	$\varepsilon_{cf}/\varepsilon_{cf\,SP01}$ (%)	$\varepsilon_{sf}/\varepsilon_{sf\,SP01}$ (%)	T/T_{SP01} (%)
SP01	100.00	100.00	100.00	100.00	100.00	100.00
SP02	109.75	109.03	112.90	89.35	105.35	112.73
SP03	109.62	118.94	108.85	108.95	94.79	114.72
SP04	109.86	120.42	107.11	98.37	87.88	118.13
SP05	109.57	117.82	107.53	101.55	101.61	109.94
SP06	111.02	127.67	106.43	105.81	104.02	121.12
SP07	110.24	120.67	117.20	100.21	110.16	137.44

Table 3: The experimental results of the tested slabs compared to those of the control specimen SP01

Failure modes

The failure of the test specimens was indicated by a significant decrease in the applied load and a large increase in the slab deflection. The failure of the tested specimens with integrated GFRP gratings was accompanied by extensive cracks as well as the visible movement of the truncated concrete cone surrounding the GFRP gratings and close to the line support. The shear cracks propagated from the column face in the specimen without gratings (specimen SP01) and around the edges of the gratings in the other specimens at varying angles to the reinforcement plane. The use of GFRP gratings resulted in an increase in the failure load and a larger punching failure surface compared to specimens without GFRP gratings (specimen SP01). Fig. 11 represents the punching failure modes of the tested specimens.

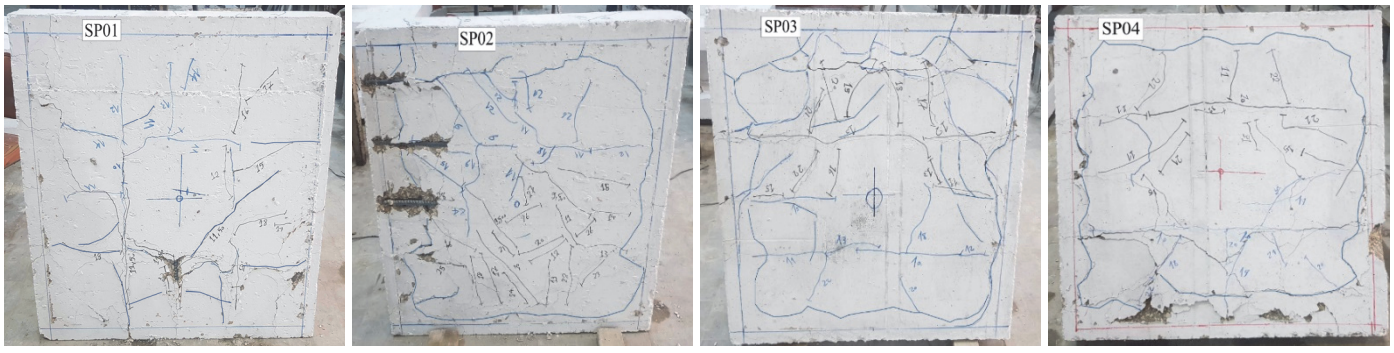

a) Specimen SP01 b) Specimen SP02 c) Specimen SP03 d) Specimen SP04

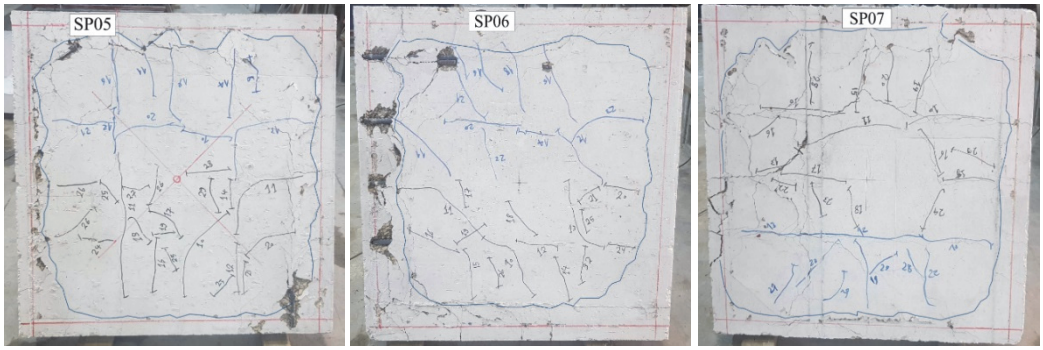

e) Specimen SP05 f) Specimen SP06 g) Specimen SP07

Figure 11: Mode of failure for the test specimens.

Load-deflection curves, failure loads, and toughness

As shown in Tab. 2 and Fig. 12, the integration of the GFRP gratings into the slab thickness of the specimens enhanced the failure load for all specimens by different percentages according to the studied parameters. Compared to the control specimen SP01 without gratings, the presence of GFRP gratings of dimensions 700×700×15 mm at the middle of the slab thickness of specimen SP02 in group 1 increased the failure load by 9.03%. For group 2, changing the location of the gratings

to the bottom of specimen SP03 and at the top of specimen SP04 throughout the slab thickness increased the failure load by 18.94% and 20.42%, respectively. Furthermore, increasing the number of GFRP gratings in group 3 with dimensions of 700×700×15 mm to two gratings attached at the top and bottom reinforcement layers of specimen SP05 increased the failure load by 17.82%. For group 4, the increase of the GFRP grating thickness to 38 mm for specimen SP06, with the same dimensions as 700×700 mm integrated at the mid-slab thickness, improved the failure load by 27.67%. Finally, for group 5, increasing the size of gratings in specimen SP07 installed at the mid-slab thickness with dimensions 800×800×15 mm increased the failure load by 20.67%. The load-deflection curves of the test specimens are presented for every group of specimens in Fig. 12. The presence of gratings in specimen SP02 increased the toughness by 12.73% compared to specimen SP01 without gratings. Calculating toughness is particularly significant for getting a good indication of the ductility of the specimens, since that indicates the specimen's capacity to withstand deformations up to failure and is equal to the area under the load-deflection curve up to the failure load. The effect of grating location enhanced the toughness by 14.72% and 18.13% for specimens SP03 and SP04, respectively, in comparison to the control specimen SP01. Doubling the number of gratings in specimen SP05 enhanced the toughness by 9.94%, which revealed a detrimental effect on the ductility behavior. For specimen SP06, increasing the thickness of the gratings resulted in a 21.12% increase in toughness. Furthermore, increasing the dimensions of the gratings resulted in a significant improvement in the toughness of 37.44%.

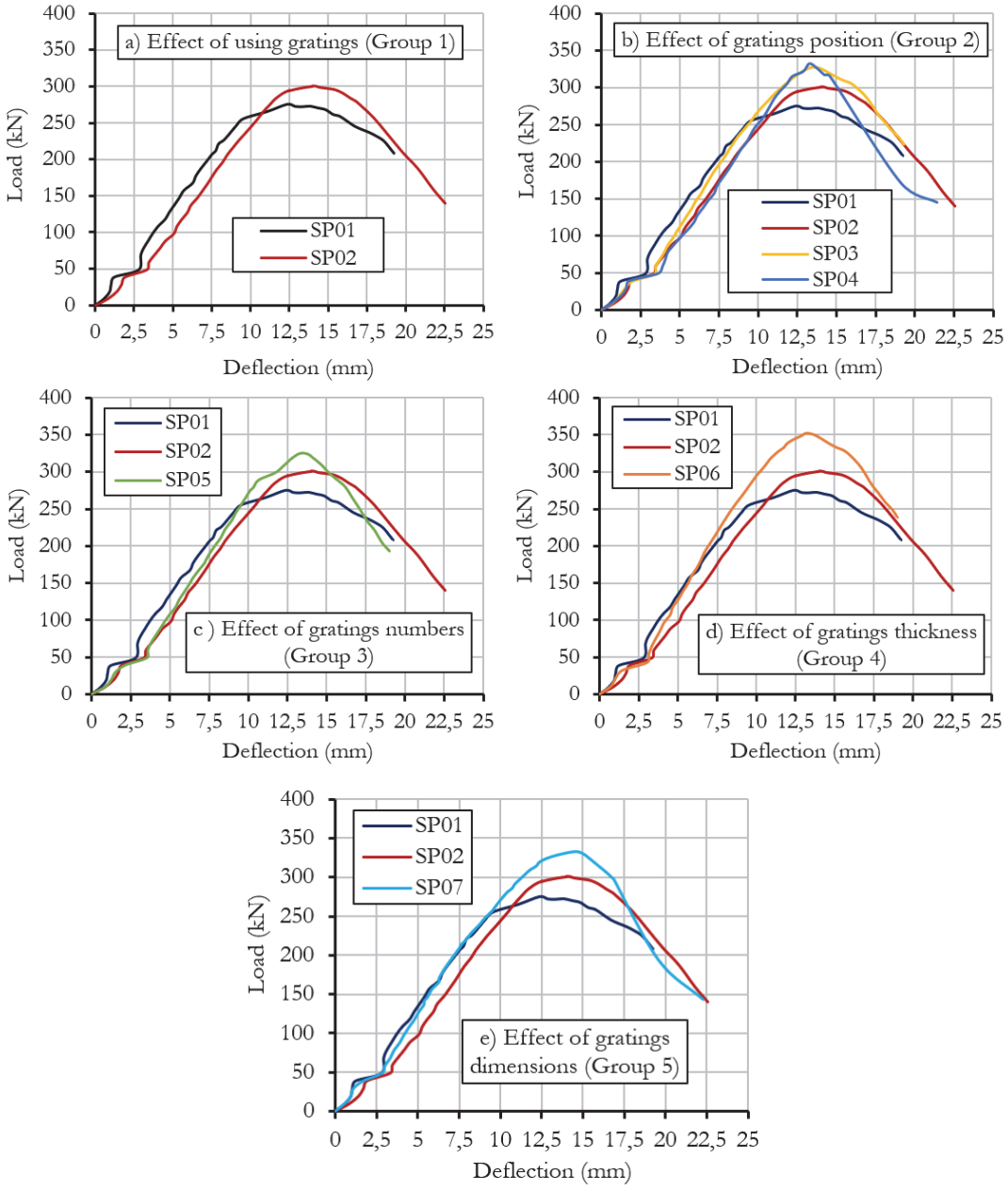

Figure 12: Load-deflection curves for the tested specimens.

Fig. 13 illustrates the first crack loads and failure loads for all the tested specimens. Figs. 14 to 16 show the bottom tension steel reinforcement strain, compressive concrete top surface strain, and grating strain for all tested specimens at the failure load. Fig. 17 shows the toughness of all tested specimens.

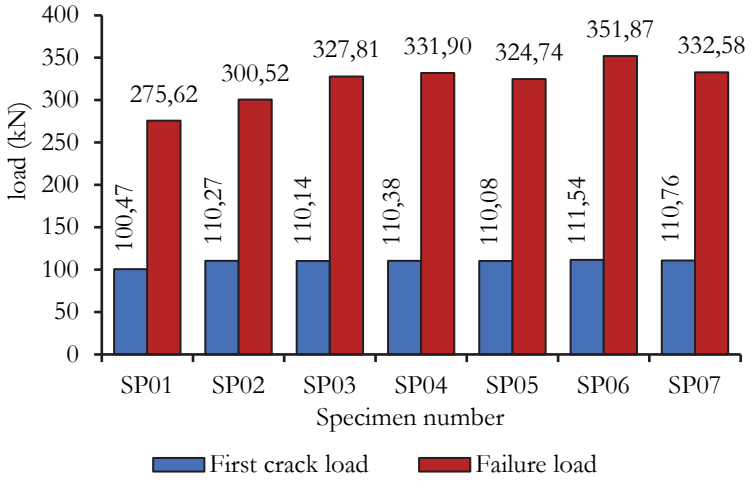

Figure 13: First crack loads and failure loads for all the tested specimens.

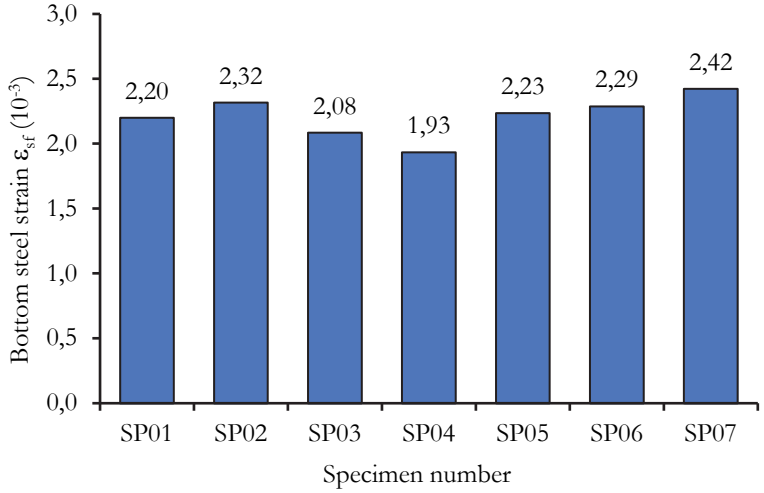

Figure 14: Bottom tension steel strain for all the tested specimens at failure load.

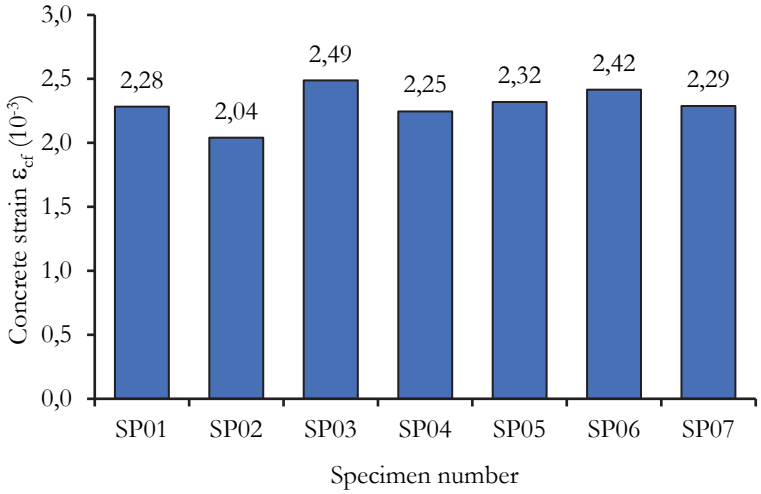

Figure 15: Concrete strain for all the tested specimens at failure load.

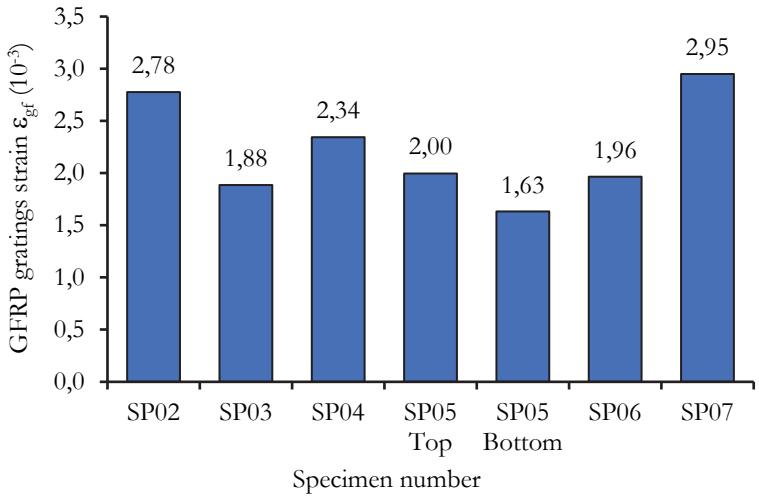

Figure 16: Gratings strain for all tested specimens at failure load.

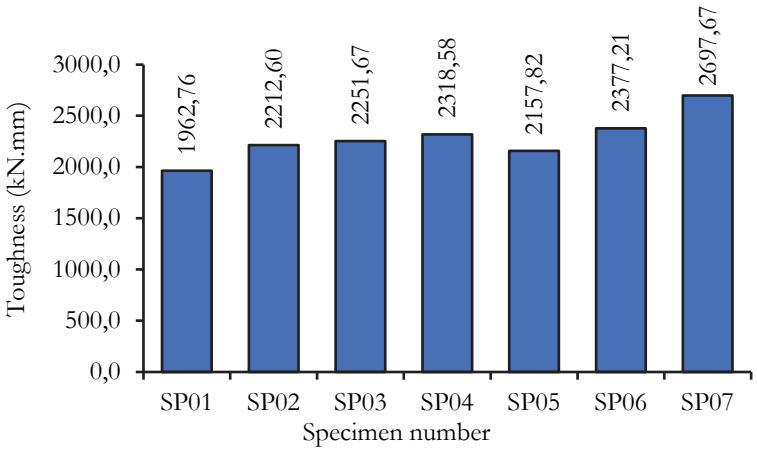

Figure 17: Toughness for all tested specimens.

NUMERICAL ANALYSIS

To compare the numerical results with the experimental ones, nonlinear finite element analysis (NLFEA) was performed by means of the ANSYS R15.0 [24] software program. A correlational investigation based on the load-deflection response, crack patterns, failure load, and failure modes was used to validate the numerical model's results with the experimental data.

Elements and boundary conditions

Using the ANSYS R15.0 technical manual [24], the concrete element was modeled using the three-dimensional isoparametric element (Solid 65). The Solid 65 element is capable of both tension and compression, cracking as well as crushing. This element is represented by eight nodal points, each of which has three translational degrees of freedom (x, y, and z) (but without rotating deformations), as well as a 2×2×2 Gaussian integration scheme used to compute the stiffness matrix of the element. The element can model concrete with a maximum of three impeded reinforcement bars that have different material properties. The steel reinforcement and GFRP gratings were modeled using the Link 180 element, which has two nodes with three transitional degrees of freedom in the X, Y, and Z directions. The connection between concrete, steel reinforcing, and GFRP gratings is considered to be a perfected bond. The translation degree of freedom in the Y direction was restrained at all nodes at the support line, and the middle nodes at the support line edge parallel to the Z axis and X axis were restrained at the X and Z translation degrees of freedom to prevent the slab from sliding and rotating on its plane.

Material modeling

The concrete material model can predict the failure of brittle materials, including both cracking and crushing failure modes. Fig. 18 shows the idealized stress-strain relationship for concrete in compression. The concrete elastic modulus (E_c), which is defined by Martinez et al. [26] in Eq. (1), is utilized. The idealized behavior of the steel bars is represented by a bilinear stress-strain curve that has two straight branches, as shown in Fig. 19. The steel reinforcing elastic modulus is represented by E_s with a value of 200 GPa. Eqns. (2) and (3) describe the relationship between the two-line segments, where ε_u is the steel reinforcement's ultimate strain = 10 ε_y; f_u is the steel reinforcement's ultimate strength that corresponds to the ultimate strain ε_u; Es is the modulus of elasticity of the steel reinforcement; and E_h is the modulus of elasticity at the second segment of the graph illustrating the strain hardening area and is assumed to be 0.1 E_s. As illustrated in Fig. 20, the stress-strain curve for the GFRP gratings is linear up to failure, where f_{gu} is the ultimate stress of the GFRP gratings; ε_{gu} is the ultimate strain of the GFRP gratings; and E_g is the modulus of elasticity of the GFRP gratings, which is equal to f_{gu}/ε_{gu}. Fig. 21 shows the experimental and numerical failure loads for all specimens.

$$E_c = 3320\sqrt{f_c'} + 6900 \text{ (MPa)} \quad (1)$$

$$f_s = E_s \varepsilon_s \qquad \varepsilon_s \le \varepsilon_y \quad (2)$$

$$f_s = f_y + Eh\,(\varepsilon_s - \varepsilon_y) \qquad \varepsilon_y < \varepsilon_s \le \varepsilon_u \quad (3)$$

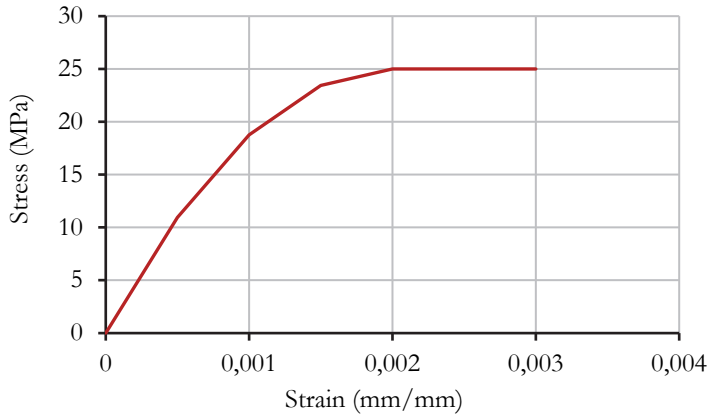

Figure 18: Idealized stress-strain curve for concrete in compression.

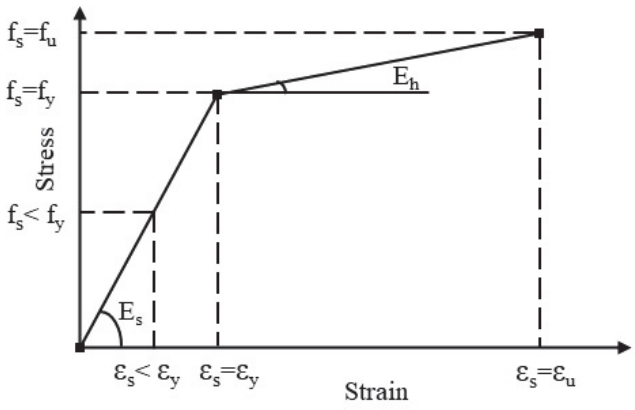

Figure 19: Bilinear stress-strain curve for steel reinforcement.

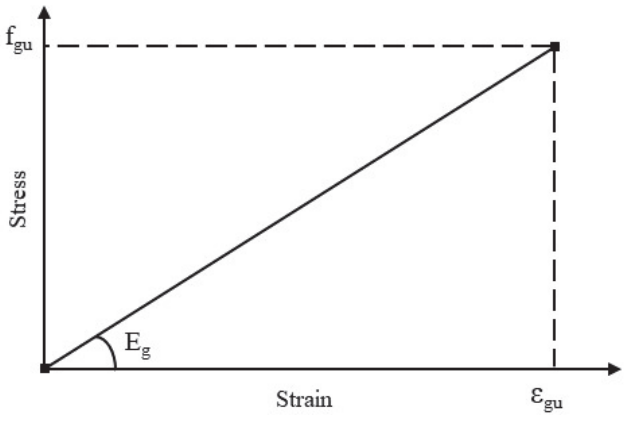

Figure 20: Stress-strain curve for GFRP gratings.

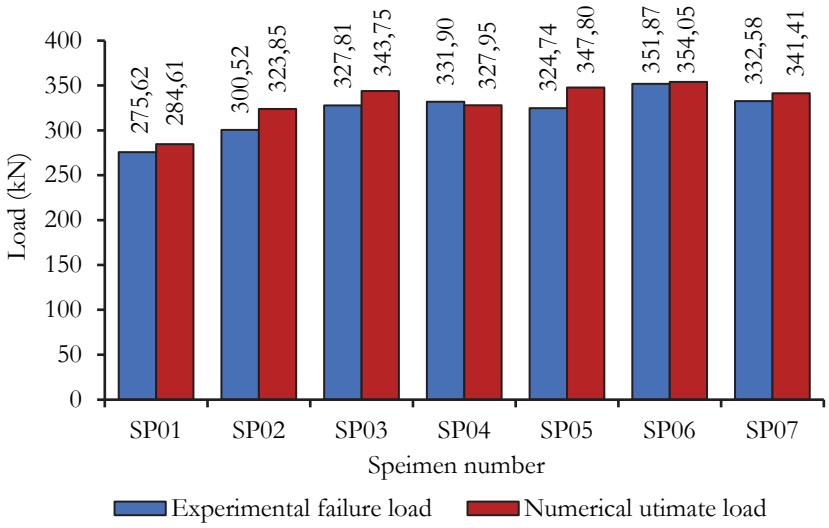

Figure 21: Experimental and numerical failure loads for all specimens.

Solution techniques

The coefficient of shear transfer for the closed crack (β_c) is widely accepted to be between 0.8 and 0.9, while the coefficient of open shear transfer (β_t) used in this study was assumed to be equal to 0.2. Nonlinear analysis was taken into account by using an incremental load process in the numerical solution scheme. Utilizing the affordably priced nature of the modified Newton Raphson method, where the stiffness is adjusted at every loading stage as used by Mahmoud A.M. [25], with the significant convergence rate of the normal Newton-Raphson technique, an iterative solution was done for each load increment. The convergence criterion utilized incremental nodal displacement, with only transitive degrees of freedom evaluated. The norm is $\psi/R \leq \phi$, where (ψ) is the iterative displacement norm and (R) is the total displacement norm. The convergence tolerance (ϕ) range of 2% to 5% produced acceptable outcomes. The analytical failure load for the test specimen was defined as the load level where the convergence requirement was not met, resulting in numerical instability.

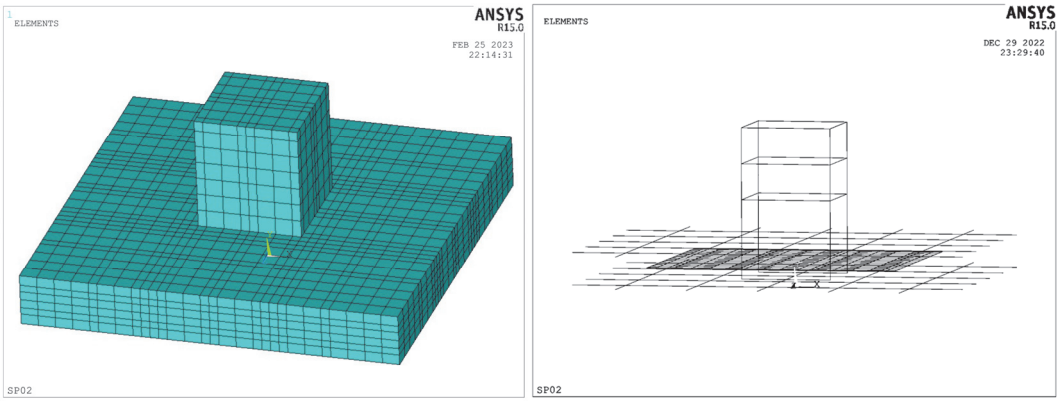

Figure 22: Idealization of concrete, reinforcement steel bars, and GFRP gratings for specimen SP02

Validation model

Fig. 22 demonstrates the typical mesh of 3-D isoparametric elements, Solid65, used to discretize all the tested slabs. Elements of six layers have been utilized to model the slab's thickness. Both the top and bottom layers reflect the top and bottom concrete covers. The slab thickness is idealized by the middle four layers. The dimensions and shape of the column stub were modeled using elements of seven layers. The slabs were considered to be simply supported along the four sides, which properly reflected the experimental setup. The steel bars and the GFRP gratings were idealized as 2-node Link 180 elements. Full bonding was assumed between the GFRP bars and the concrete elements. The model was meshed to account for all the grating positions and the studied dimensions used in the experimental study. In addition, the location of the top and bottom steel reinforcement layers, vertical reinforcement, and column stirrups was considered. Setting the boundary's condition was simple. The Y translation degree of freedom was constrained at all nodes along the support line, and the X

and Z translation degrees of freedom were constrained at the center nodes along the support line edges parallel to the Z axis and X axis to prevent the slab from sliding in its plane.

Comparison of experimental and numerical results

Numerical results using the "ANSYS R15.0" [24] software conform to those recorded experimentally, as shown in Figs. 23 and 24. It had been observed that the NLFEA load deflection relationship slopes extensively steeper than experimental results. The slab stiffness overestimation may be attributed mostly to the finite element idealization and, to a lesser extent, to the Young's modulus of concrete used in the current study. The concrete elastic modulus (E_c) may be overstated. The use of six layers to represent the slab thickness may have resulted in a stiffer slab model than the actual slab specimen. Furthermore, the predicted cracking loads (N_{cr}) are in general less than the observed experimental cracking loads (P_{cr}), with a mean N_{cr}/P_{cr} ratio of 0.71 and a coefficient of variation (C.O.V.) of 0.05. This can be attributed to the concrete cracking strength employed in the NLFEA, which, according to ACI provisions, may have been overestimated, or to the production of invisible cracks in the specimen during the experimental operations. Furthermore, the cracking strength of concrete was assumed to be 10% of the concrete compressive strength, which may result in an underestimation of cracking loads. Also, the numerical first crack is an internal crack in the direction perpendicular to the tension principal stress in concrete, which is not visible in the experimental test and occurred at a load less than the external visible experiment crack. The NLFEA results, on the other hand, show good agreement between the experimental and numerical results for the load-deflection curves, crack patterns, and failure loads, within a difference varying between 1.0% and 8.0% for the ultimate load, as shown in Tab. 4, which is acceptable.

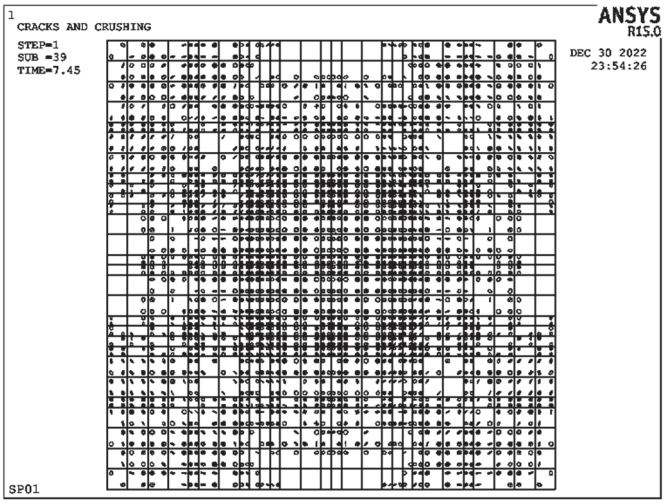

Specimen SP01

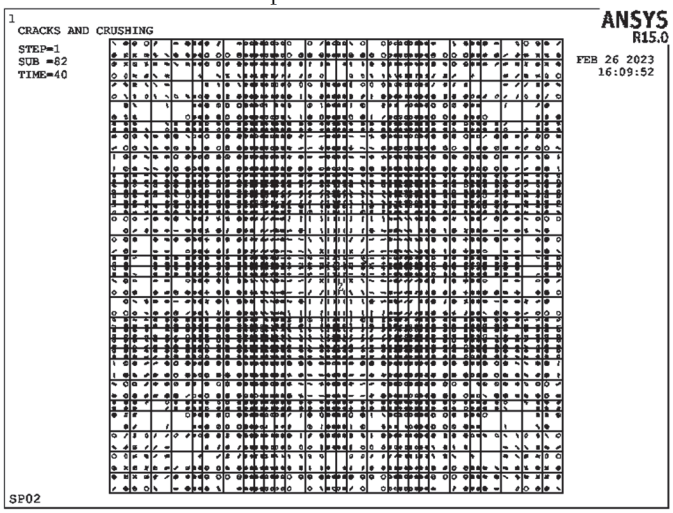

Specimen SP02

Figure 23: Numerical crack patterns for specimens SP01 and SP02.

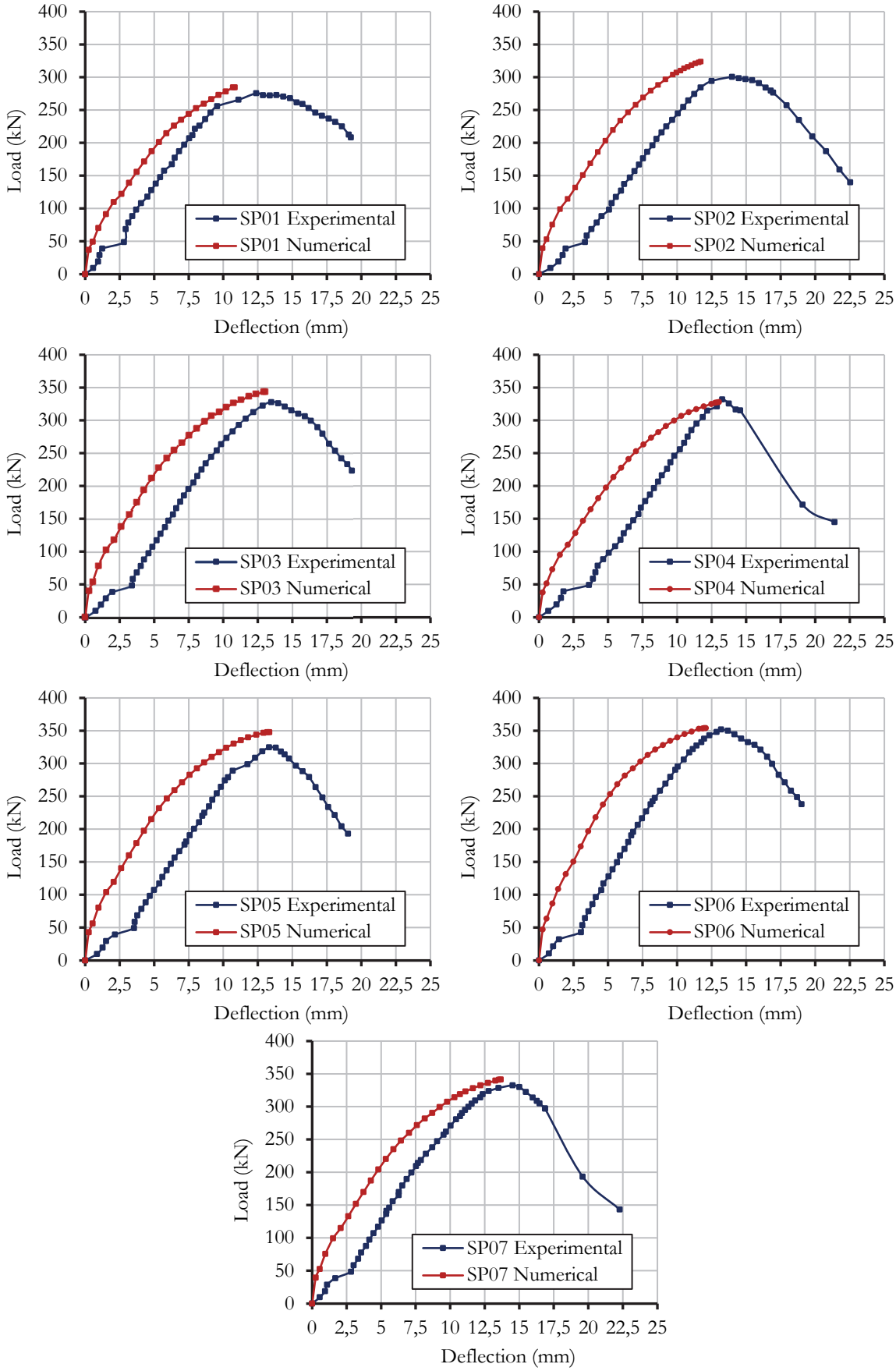

Figure 24: Experimental Vs predicted load–deflection curves for all the tested specimens.

Specimen Number	Experimental results			NLFEA results			NLFEA / Exp.		
	First crack load P_{cr} (kN)	Failure load P_f (kN)	Deflection at failure load $\Delta_{f\,exp}$ (mm)	First crack load N_{cr} (kN)	Ultimate load N_u (kN)	Deflection at ultimate load $\Delta_{u\,num}$ (mm)	N_{cr} / P_{cr}	N_u / P_f	$\Delta_{u\,num}$ / $\Delta_{f\,exp}$
SP01	100.47	275.62	12.39	70.35	284.61	10.84	0.70	1.03	0.87
SP02	110.27	300.52	13.98	75.37	323.85	11.72	0.68	1.08	0.84
SP03	110.14	327.81	13.48	78.83	343.75	13.03	0.72	1.05	0.97
SP04	110.38	331.90	13.27	72.87	327.95	13.03	0.66	0.99	0.98
SP05	110.08	324.74	13.32	80.36	347.80	13.33	0.73	1.07	1.00
SP06	111.54	351.87	13.18	86.65	354.05	12.08	0.78	1.01	0.92
SP07	110.76	332.58	14.52	75.54	341.41	13.66	0.68	1.03	0.94
Mean value							0.71	1.04	0.93
Standard deviation							0.04	0.03	0.06
C.O.V.							0.05	0.03	0.06

Table 4: Comparison of test results with NLFEA from ANSYS.

Conclusions

This study presents a proposal for a new reinforcing system to improve the punching shear resistance of flat slab column connections with integrated GFRP gratings. Based on the experimental findings and numerical results of this study, the following points can be concluded for the range of studied parameters:

1- Specimens provided with GFRP gratings exhibited larger punching shear perimeters than the control specimen without a significant change in the cracking pattern. Therefore, the use of the proposed GFRP grating system enhances the behavior of RC flat slabs.
2- An enhancement in the failure load was recorded for specimens provided with the suggested GFRP gratings. The enhancement ranged from 9.03% to 27.67%.
3- The presence of GFRP gratings at the mid-slab thickness increased the failure load by 9.03%.
4- Changing the location of the gratings to the bottom and the top throughout the slab thickness increased the failure load by 18.94% and 20.42%, respectively, compared to the mid-slab position.
5- Using two GFRP gratings with the same dimensions attached to the top and bottom reinforcement layers of the slab increased the failure load by 17.82% compared to the control specimen.
6- Using the GFRP grating with a thickness of 38 mm at the mid-slab thickness improved the failure load by 17.13% compared to the control specimen.
7- Increasing the dimensions of the gratings by 15% when installed at the mid-slab thickness increased the failure load by 27.67% compared to the control specimen.
8- For the range of the studied parameters, all the specimens failed in a punching shear mode with a brittle manner and a sudden loss of capacity. The use of GFRP gratings resulted in a wider punching failure surface than that of the specimen without the suggested gratings.
9- The maximum recorded compressive concrete and bottom tension steel strains for the specimens were 0.0025 and 0.0024, respectively, which means that steel reinforcement reaches the yield point while GFRP gratings do not reach the failure strain.
10- The grating strains for all specimens with a thickness of 15 mm and 38 mm do not exceed the maximum grating strain at failure of 0.003 and 0.0053, respectively, as determined by the experimental load-bearing test.
11- Using the suggested grating enhanced the test specimen's toughness, which ranged from 9.94% to 37.44% compared to the control specimen.
12- The application of the nonlinear finite element method yielded superior results, including crack patterns, load carrying capacity, and load-deflection response.
13- Numerical results are found to be in good agreement with those obtained experimentally, within a difference of 1.0% to 8.0% for the failure load.

REFERENCES

[1] Bank, L.C., Xi, Z. and Munley, E. (1992). Tests of full-size pultruded FRP gratings reinforced concrete bridge decks. Conference Proceedings of ASCE, Materials Engineering Congress, New York, pp. 618-631.

[2] Biddah, A. (2006). Structural reinforcement of bridge decks using pultruded GFRP gratings. Composite Structures, 74, pp. 80-88. DOI: 10.1016/j.compstruct.2005.03.016.

[3] Bank, L.C., Frostig, Y. and Shapira, A. (1997). Three-dimensional FRP grating cages for concrete beams. ACI Structural Journal, (94) 6, pp. 643-652. DOI: 10.14359/9724.

[4] Gattesco, N., Dilena, M. and Boem, I. (2019). Experimental and numerical study on the bending performances of glass FRP-molded gratings: Influence of restraining conditions and cover plates. Composite Structures, 223, p. 110967. DOI: 10.1016/j.compstruct.2019.110967.

[5] Swamy, R. N. and Ali, S. A. R. (1982). Punching shear behavior of reinforced slab-column connections made with steel fiber concrete. ACI Structural Journal, (79) 5, pp. 392-406. DOI: 10.14359/10917.

[6] Ospina, C. E., Alexander, S. D. B. and Cheng, J. J. R. (2003). Punching of two-way concrete slabs with fiber-reinforced polymer reinforcing bars or grids. ACI Structural Journal, (100) 5, pp. 589-598. DOI: 10.14359/12800.

[7] Mu, B. and Meyer, C. (2003). Bending and punching shear strength of fiber-reinforced glass concrete slabs. ACI Structural Journal, (100) 2, pp. 127-132. DOI: 10.14359/12552.

[8] Zhang, B., Masmoudi, R. and Benmokrane, B. (2004). Behavior of one-way concrete slabs reinforced with CFRP grid reinforcements. Construction and Building Materials, 18, pp. 625-635. DOI: 10.1016/j.conbuildmat.2004.04.007.

[9] Dimitrios, D., Theodorakopoulos, H. and Swamy, N. (2007). Analytical model to predict punching shear strength of FRP-reinforced concrete flat slabs. ACI Structural Journal, (104), 3, pp. 257-266. DOI: 10.14359/18615.

[10] Esfahani, M. R., Kianoush, M. R. and Moradi, A. R. (2007). Punching shear strength of interior slab column connections strengthened with carbon fiber-reinforced polymer sheets. Engineering Structures, (31) 7, pp. 1535-1542. DOI: 10.1016/j.engstruct.2009.02.021.

[11] Said, M., Adam, M.A., Arafa, A.E. and Moatasem, A., (2020). Improvement of the punching shear strength of reinforced lightweight concrete flat slabs using different strengthening techniques. Journal of Building Engineering 32, 101749. DOI: 10.1016/j.jobe.2020.101749.

[12] Hemzah, S. A., Al-Obaidi, S. and Salim, T. (2019). Punching shear model for normal and high-strength concrete slabs reinforced with CFRP or steel bars. Jordan Journal of Civil Engineering, (13) 2, pp. 250-268.

[13] Kim, M. S. and Lee, Y. H. (2021). Punching shear strength of reinforced concrete flat plates with GFRP vertical grids. Applied Sciences, (11) 6, DOI: 10.3390/app11062736.

[14] Mohmmad, S.H., Gülşan, M..E. and Çevik, A. (2022). Punching shear behavior of geopolymer concrete two-way slabs reinforced by FRP bars under monotonic and cyclic loadings. Journal of Advances in Structural Engineering, (25) 3, DOI: 10.1177/13694332211052349.

[15] Mahmoud, A. A., Said, M,. and Salah, A. (2016). Nonlinear finite element analysis for reinforced concrete slabs under punching loads. International Journal of Civil Engineering & Technology (IJCIET), (7), 3, pp. 392–397.

[16] Said, M., Mahmoud, A. A. and Salah A. (2020). Performance of reinforced concrete slabs under punching loads. Journal of Materials and Structures, (53) 4, DOI: 10.1617/s11527-020-01509-5.

[17] Nguyen, M., L. and Rovňák, M. (2013). Punching shear resistance of interior GFRP-reinforced slab-column connections. Journal of Composites for Construction, 17(1), pp.2-13. DOI: 10.1061/(ASCE)CC.1943-5614.0000324.

[18] Elmoien, Y. A., Mahmoud, A. A., El-Mahdy, O. and Salah, A. (2022). Proposed Correction factors for punching shear capacity of RC flat slabs with shear reinforcement. Engineering Research Journal (ERJ), (51), 4, pp. 8-18. DOI: 10.21608/erjsh.2022.151469.1065.

[19] ACI Committee 318 (2019). Building Code Requirements for Structural Concrete (ACI 318-19). An ACI Standard, Commentary on Building Code Requirements for Structural Concrete (ACI 318R-19), American Concrete Institute.

[20] ASTM, D790-02 (2002). Standard test methods for the flexural properties of unreinforced and reinforced plastics and electrical insulating materials. ASTM International, West Conshohocken, PA, USA.

[21] ASTM, C496/C496M-14 (2014). Standard test method for static modulus of elasticity and Poisson's ratio of concrete in compression. ASTM International, West Conshohocken, PA, USA.

[22] ASTM, C496/C496M-17 (2017). Standard test method for splitting the tensile strength of cylindrical concrete specimens. ASTM International, West Conshohocken, PA, USA.

[23] ASTM, C39/C39M-21 (2021). Standard test method for compressive strength of cylindrical concrete specimens. ASTM International, West Conshohocken, PA, USA.

[24] Manual, F.L.U.E.N.T. (2012). ANSYS Release Version 15.0. User's Guide.

[25] Mahmoud, A.M. (2015). Finite element implementation of punching shear behaviors in shear-reinforced flat slabs. Ain Shams Engineering Journal, 6(3), pp. 735-754. DOI: 10.1016/j.asej.2014.12.015.
[26] Martinez, S., Nilson, A. H. and Slate, F. (1984). Spirally reinforced high-strength concrete columns. ACI Structural Journal, (81) 5, pp. 431-442. DOI: 10.14359/10693.

NOMENCLATURE

P_{cr} : Experimental first crack load;
N_{cr} : Numerical first crack load;
P_f : Experimental failure load;
N_u : Numerical ultimate load;
$\Delta_{f\,exp}$: Experimental deflection at mid-span at failure load;
$\Delta_{u\,num}$: Numerical deflection at mid-span at ultimate load;
ε_{cf} : Concrete compressive strain at failure load;
ε_{sf} : Bottom reinforcement steel strain at failure load;
ε_{gf} : GFRP gratings strain at failure load;
T : Toughness, which is the ability to adsorb deformations up to failure and equals the area under the load-deflection curve up to failure;
$f_c`$: Average concrete cylinder compressive strength; and
f_y : Reinforcement yield strength.